Defect clustering during ion irradiation of GaAs: Insight from molecular dynamics simulations

K. Nordlund,[a] J. Peltola, J. Nord, and J. Keinonen
Accelerator Laboratory, P.O. Box 43, FIN-00014 University of Helsinki, Finland

R. S. Averback
Materials Research Laboratory, University of Illinois, Urbana, Illinois 61801

(Received 14 December 2000; accepted for publication 16 May 2001)

Defect formation in compound semiconductors such as GaAs under ion irradiation is not as well understood as in Si and Ge. We show how a combination of ion range calculations and molecular dynamics computer simulations can be used to predict the atomic-level damage structures produced by MeV ions. The results show that the majority of damage produced in GaAs both by low-energy self-recoils and 6 MeV He ions is in clusters, and that a clear majority of the isolated defects are interstitials. Implications of the results for suggested applications are also discussed. © *2001 American Institute of Physics.* [DOI: 10.1063/1.1384856]

I. INTRODUCTION

Gallium arsenide is a widely used semiconductor material that offers decisive advantages to silicon and germanium for some opto-electronic applications.[1] Because ion implantation is usually the best means to introduce dopants into materials in a controlled manner, the interest in understanding the effects of ion irradiation in GaAs is important for the further development of controlled manufacturing of GaAs components.

Molecular dynamics (MD) simulations are well known to be the best method for studying irradiation processes on an atomistic level,[2–8] but few studies have, to date, examined irradiation effects in GaAs, and even those have been limited to quite low energies.[5,9] In large part, this is because the GaAs classical interatomic potentials have been poor in describing nonequilibrium phenomena.[10] We have recently developed a GaAs potential[11] which overcomes many of the hurdles posed by the previous potentials. While the point defect properties predicted by our classical potential may still not be fully reliable (see Sec. II C and Ref. 8), it can be expected to reliably predict the overall distribution of the damage, the division of the damage into point defects and defect clusters, and the size of amorphous zones.

Transmission electron microscopy (TEM) experiments have unequivocally shown that heavy ion irradiation at keV energies produces large damage clusters in GaAs.[12,13] However, the TEM experiments can not see individual defects or very small clusters. Although several other experimental methods can observe point defects, these again do not usually give clear information on cluster properties. The binary collision approximation (BCA) simulations most commonly used in the field are also not very good at predicting defect cluster production as they can not describe multiple simultaneous collisions in a small spatial region.

Since cascade simulations performed with classical MD should be reliable in predicting how defects are divided into point defects and defect clusters, they are a good tool for obtaining a better understanding of defect clustering during the ion irradiation of GaAs.

In this article, we study this problem in two energy regimes. We first (Sec. III A) study the damage produced by low-energy (0.4–10 keV) self-recoils in bulk GaAs. The energy of 10 keV is chosen as a maximum because (as we shall show) it is above the energy where cascades are split into subcascades. While this case is not directly related to any common experimental situation, the information gained can be used to understand damage produced by high-energy ions, neutrons, or electrons producing recoils in GaAs. To demonstrate this, we evaluate, in Sec. III B, the damage produced by 100 keV H and 6 MeV He ions irradiating thin layers of GaAs.

These particular irradiation conditions are of practical interest in space physics applications. Satellites in near-earth orbit are usually powered by GaAs-based solar cells, which are bombarded by cosmic rays which contain protons with energies of the order of 100 keV.[14] Radio-isotopes emitting ~6 MeV α particles could produce electron–hole pairs in GaAs, and thus have been considered as a potential power source in space probes traveling far from the sun. However, because the protons and α particles produce damage in GaAs, it is important to know how much damage is produced, and be able to estimate how much of it is in defects which are difficult to anneal out.

II. METHOD

A. Collision cascade simulations

To simulate collision cascades in bulk GaAs, we use the same approach as discussed in detail in Ref. 8. A Ga or As atom close to the center of a simulation cell with periodic boundaries in all directions is initially given a recoil energy in a randomly chosen direction. The evolution of the resulting collision cascade is then followed until no significant atom motion is observed in the cell. Heat generated by the

[a]Electronic mail: kai.nordlund@helsinki.fi

cascade event is removed from the simulation cell at the outer boundaries using Berendsen temperature control[15] with a time constant optimized to dissipate heat efficiently. The ambient temperature was 0 K, but test simulations at 300 K showed that the results do not change significantly as long as the temperature is much below the melting temperature. The Ziegler–Biersack–Littmark (ZBL) electronic stopping model was applied as a frictional force on all atoms with a kinetic energy above 5 eV.

The parameters and basic features of the interatomic potential used in these simulations is given in Appendix A; additional details will be given elsewhere.[11]

Defects were recognized in the cells using Wigner–Seitz cells and spheres centered on lattice sites, and by detecting atoms with a potential energy at least 0.2 eV above the equilibrium value. The difference between these defect calculation schemes has been examined in detail in Ref. 8 for Si; we found that the same qualitative features are valid also for GaAs. For compatibility with the previous article, we used Wigner–Seitz defects in our defect cluster analysis. We used a cutoff radius r_{cl} of 1 lattice constant (about 5.65 Å) for determining whether two defects are part of the same cluster; comparison with visual inspections of defect structures produced in several cascades showed that this cutoff value gave cluster sizes in good agreement with an intuitive picture obtained in the visual inspection.

Since a split interstitial structure containing two different atom types should not be counted as an antisite, we used spheres with a radius of 1 Å centered on a lattice sites to detect antisite defects. Because detection of an antisite in an amorphous zone is not meaningful, we report antisite results only for cells where the amorphous zones have been annealed by rapid heating.

B. High-energy ions

The energy deposition and integrated primary recoil spectrum generated by high-energy ions was obtained using the MDRANGE code.[16] The ranges were calculated using the universal ZBL repulsive potential,[17] the SRIM96[18] electronic stopping power, and including the straggling of the electronic stopping[19] in the simulation. A ''random'' irradiation direction (7° off the ⟨100⟩ crystal direction, with a random rotation angle around the axis) was employed, with the range evaluated as the final z coordinate of the ions.

The code was used to generate statistics of the number of primary recoils produced at a given energy per incoming ion, i.e., the integrated primary recoil spectrum $n_t(E)dE$, where t is the atom type. If the damage production by a given self-recoil $N_t^D(E)$ is known from the full MD simulations, the total damage produced for the implantation N_{tot}^D can then be evaluated as

$$N_{\mathrm{tot}}^D = \sum_{t=1}^{N_t} \int_{E_{\mathrm{thres}}}^{E_0} N_t^D(E) n_t(E) dE, \tag{1}$$

where N_t is the total number of atom types, E_{thres} a threshold displacement energy, and E_0 the initial implantation energy. In practice, it is enough to integrate up to the maximum possible energy transfer since $n_t(E) \equiv 0$ above this energy.

This approach involves two approximations. The first is the assumption that the recoils are produced so well separated from each other that the resulting cascades are nonoverlapping. For MeV light ions, this is a very good approximation. The other approximation is a bit more severe. It assumes that the directions of the recoils do not on average affect the amount of damage produced. For irradiation in a random (as opposed to channeling) crystal direction, we have reason to believe that this is a good approximation; in recent simulations of full amorphization of Si, Ge, and GaAs we found that the results are independent of the direction of the recoils.[20]

In this particular case, due to the irradiation of GaAs, we can introduce one more approximation. Since Ga and As have almost the same mass and equivalent lattice positions, we can assume that the total damage production for energies well above the displacement energy threshold is the same, i.e., $N_{\mathrm{As}}^D(E) = N_{\mathrm{Ga}}^D(E)$.

C. Method reliability

The range calculation method has been tested against experimental results numerous times (e.g., Refs. 21–23), and found to be quite accurate in all cases where the stopping is either dominated by nuclear stopping, or where the electronic stopping is well known. The case of MeV He irradiation can be considered to belong to the latter category.

The full collision cascade simulations are not necessarily as accurate. In particular, the properties of individual point defects or small defect clusters predicted by the classical potential can not be considered reliable without comparison to quantum mechanical calculations or experiments. Since the point defect production in cascades depends strongly on the defect formation energy, the detailed structure of the point defects produced in the cascades should be viewed with caution. We will examine the detailed properties of point defects produced in cascades in GaAs in a forthcoming paper.[24]

However, there are still several features which we believe can be determined reliably. Many of the interstitials produced in the cascades are the results of energetic ($E_{\mathrm{kin}} > 10$ eV) collisional events, which can be expected to be treated well by the potential since it has a reliable repulsive part. In Si, we have earlier demonstrated that the fraction of damage in interstitials far from other damage is indeed roughly independent of the choice of the interatomic potential.[8]

In GaAs, we have also performed some comparison between potentials. Comparison of cascades in realistic GaAs and GaAs, where the chemical difference between the constituents was removed, gave almost exactly the same total amount of damage.[25] Comparison of the damage production in 1 keV GaAs modeled by our potential and the potential of Sayed[9,10] showed that the Sayed model gives about 35% lower damage numbers. This indicates the level of uncertainty of the calculation. Since our potential fit has a better description of nonequilibrium, liquid, and solid states, however, the present results should be considered more reliable.

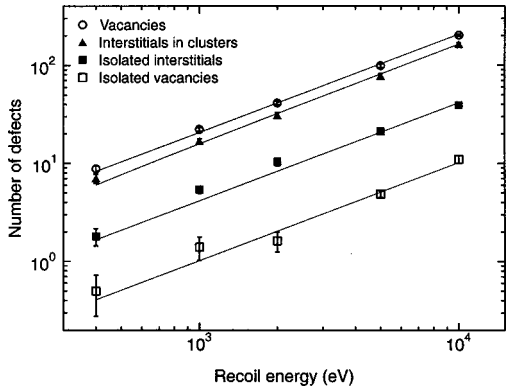

FIG. 1. Damage produced by self-recoils in GaAs is shown. The amount of vacancies in clusters and total amount of interstitials is left out since these curves overlap almost exactly with that for the total amount of vacancies. The lines are fits of a linear function to each data set.

Finally, we shall see next that the effective displacement energy found in our simulations agrees well with that commonly used in simple estimates of damage in GaAs. From this discussion, we conclude that although the exact structure of point defects produced in cascades may not be reliably predicted by our model, the division of damage into free and clustered defects, and the total amount of damage produced, can be expected to be predicted well.

III. RESULTS

A. Collision cascades

The average numbers of isolated interstitials, isolated vacancies, interstitials in clusters, and total vacancies are shown in Fig. 1. The number of vacancies in clusters and total interstitials is left out of Fig. 1 since these overlap almost exactly with the curve for the total number of vacancies. No statistically significant difference in the damage production was observed between Ga and As recoils.

The lines are fits of a linear function $y=a(E-E_{\text{thres}})$ to the data. For the number of defects in clusters, we used MD simulations to determine the minimum energy at which a defect cluster (containing more defects than a single Frenkel pair) can be produced, obtaining $E_{\text{thres}}\approx 30$ eV. This value was used in the fits to all clustered defect curves. For the number of isolated and total defects, we tried fits with a nonzero threshold E_{thres}, but the fitting parameter E_{thres} was found to be 0 within the uncertainties, so we used $E_{\text{thres}}=0$ in the final fits. Note that using a value of 0 agrees with the simple Kinchin–Pease theory.[26]

Several interesting features can be deduced from Fig. 1. The fits show that except possibly for the case of isolated interstitials, the data follow linear behavior. For free interstitials, the 1 and 2 keV points appear to deviate from the linear behavior; However, the deviation is within the statistical fluctuation.

We note that since all damage is produced by the nuclear deposited energy, the linearity with the recoil energy will be valid only as long as the nuclear deposited energy F_{D_n} is a linear function of the recoil energy E. We checked that this is true for at least up to 10 keV. Examination of stopping power curves showed that the linear dependence can be expected to be a good approximation to energies of about the nuclear stopping power maximum at ~40 keV. As we shall see below, most damage for the high-energy irradiation is produced by recoils well below 40 keV, so we shall use the approximation $F_{D_n}\propto E$ for simplicity.

We also see that the vast majority of the damage is in clusters at all energies. While this is not surprising for the 5 and 10 keV energies, since it is well known that at these energies large amorphous clusters are produced, it may be somewhat surprising that even at the low energies around 400 eV, the fraction of damage in clusters is quite high. The free defects are predominantly interstitials. This is simply because interstitials can be easily produced far from other damage by ballistic recoils or replacement-collision sequences, but for vacancies this is much less likely at the relatively low energies involved here

The distribution of damage in clusters is further examined in Table I and Fig. 2. Table I shows that there is no significant difference between the fraction of damage in clusters for 5 and 10 keV recoils, and even the 2 keV data are quite close to the 5 keV one. However, the 1 keV cluster size distribution does not contain very large clusters (more than 40 defects). This shows that between 2 and 5 keV the cascade structure becomes self-similar due to subcascade formation, with little difference in the *average* damage distribution. However, even though below a cluster size of about 60 defects, the 2 and 5 keV distributions are similar in shape,

TABLE I. Fraction of isolated and clustered Wigner–Seitz defects in GaAs cascades is shown. Note that the results depend somewhat on the choice of the value of r_{cl} (see discussion in text); the value used here was one unit cell. N_{def} is the total number of defects in each case. F^{isol} gives the fraction of isolated defects, F_i^{isol} the fraction of isolated interstitials and F_v^{isol} the fraction of isolated vacancies compared to the total number of defects. F^{clus}, F_i^{clus}, and F_v^{clus} give the fraction of defects, interstitials, and vacancies, respectively, in clusters with at least six defects. All fractions are given as percents of the total number of defects; since clusters with a size of two to five defects are not included, the total does not equal 100%.

Energy (keV)	N_{def}	F^{isol} (%)	F_i^{isol} (%)	F_v^{isol} (%)	F^{clus} (%)	F_i^{clus} (%)	F_v^{clus} (%)
0.4	18±1	13.1±0.7	10.2±0.7	2.8±0.4	43±4	18±2	25±2
1	45±2	15.2±0.4	12.1±0.3	3.1±0.3	64±2	27±1	37±1
2	83±34	14.5±0.4	12.5±0.4	2.0±0.2	58±3	24±2	33±2
5	198±9	13.2±0.2	10.7±0.2	2.5±0.1	60±2	25±1	34±1
10	397±10	12.6±0.2	9.9±0.2	2.7±0.1	60±1	26±1	33±1

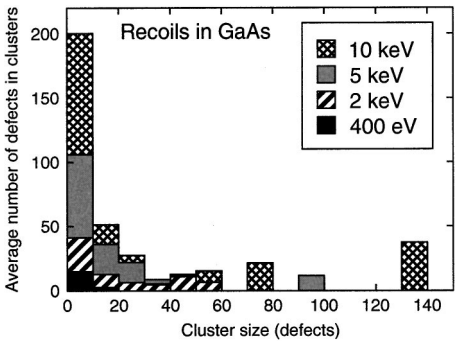

FIG. 2. Distribution of Wigner–Seitz defects as a function of the cluster size, measured as the number of defects each cluster contains is shown. The data for each energy is overlaid on that of the higher energies. The 1 keV results have been omitted for clarity. The numbers are the average over six to ten events for each energy. Note that because of the limited number of events and clusters produced by them, the upper end of the 5 and 10 keV distributions, above about 50 defects, are not statistically significant, as the data reflects defects in single clusters produced in a single event.

the 5 and 10 keV events produce very large damage clusters (sizes above 60 defects in a cluster) in a few isolated instances. Taken together, the data illustrate that a few very dense cascades can produce increasingly large clusters up to energies of at least 10 keV, but that this is not reflected in the average division of damage into clustered and isolated defects.

Final damage distributions for two 10 keV events, one with the least damage production, and one with the most, are illustrated in Fig. 3. We see that the vast majority of the damage is indeed in large amorphous clusters, as expected from the previously described analysis. Furthermore, even though we chose the two events with the least and most damage for Fig. 3, we see that the overall shape and size of the damaged regions are quite similar.

B. Damage production by high-energy irradiation

The damage produced in GaAs by 100 keV H and 6 MeV He irradiation was examined with the method described in Sec. II B. Since we found that the damage production is to a very good approximation linear with energy, we used the linear fits to give $N_D(E)$ for an arbitrary energy. A value of 15 eV was used for E_{thres} for isolated defects and 30 eV for clustered defects. The results were found to be insensitive to the exact value of E_{thres} since most damage was produced by higher-energy recoils. Here, we will present the analysis for 6 MeV He ions in detail. The analysis for 100 keV H ions was carried out exactly as the analysis for 6 MeV He ions which considered the whole depth range.

The total nuclear deposited energy as a function of depth $F_{D_n}(z)$ for 6 MeV He is shown in Fig. 4. Figure 4 shows that between 0 and 14 μm, the nuclear deposited energy distribution is essentially constant with $F_{D_n} \approx 0.67$ keV/μm. This depth region could be interesting for the application discussed in the introduction, since the amount of electronic excitation is high in this region while damage production is low.

We therefore consider two cases in the remaining analysis: damage between 0 and 10 μm and the total damage production over all z. To obtain the damage between 0 and 10 μm, we used a recoil spectrum calculated between 2 and 10 μm (to avoid possible surface effects). Tests of calculating recoil spectra in different intervals between 0 and 10 μm showed that the recoil spectrum is similar in shape in the whole interval, and the absolute defect numbers obtained in the analysis anywhere in the interval vary by less than 20% from the average calculated between 2 and 10 μm. For easy interpretation for thin GaAs layers of different thicknesses, we report the damage in the surface region as damage per 1 μm depth.

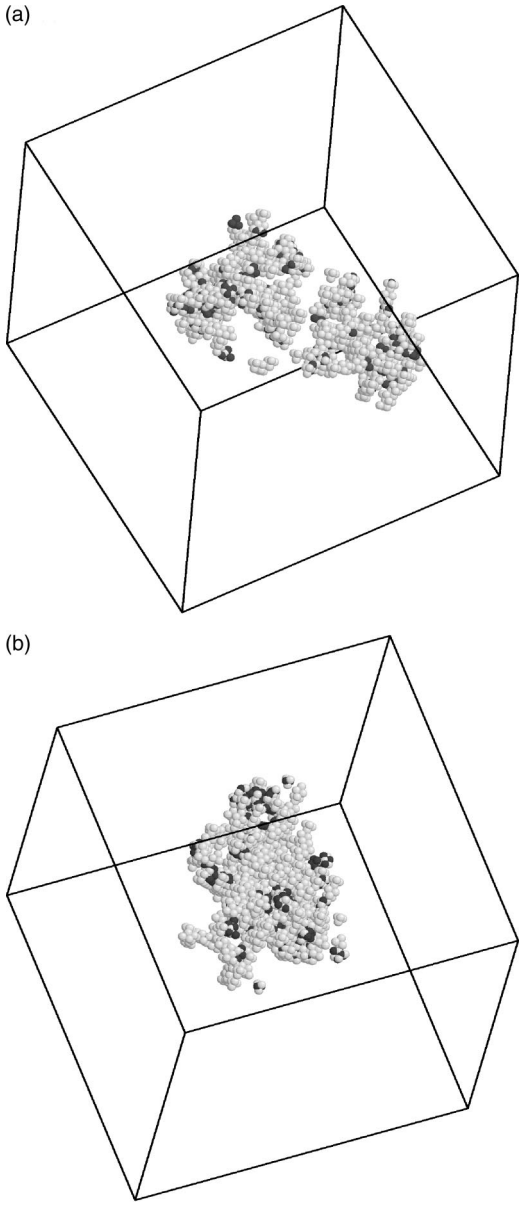

FIG. 3. Defect clusters produced in two 10 keV defects in GaAs are presented. Shown are the positions of all atoms with a potential energy at least 0.2 eV higher than the equilibrium value, with Ga atoms shown as darker and As atoms as the lighter spheres. The black lines show the sides of the cubic simulation cell; the side length is 203.5 Å. (a) Shows the 10 keV event where most damage was produced, and (b), the event with least damage. Note that because of the three-dimensional nature of the damage, the damage is in fact divided into more clusters than what appears. Still, we illustrate that the damage produced is concentrated in a few large amorphous clusters.

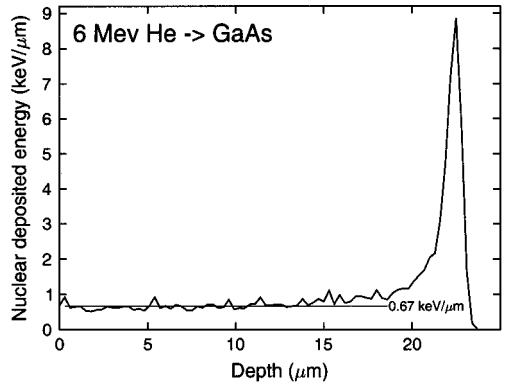

FIG. 4. Nuclear deposited energy as a function of depth for 6 MeV He irradiation of GaAs is shown. The thin line shows the deposited energy level of 0.67 keV/μm.

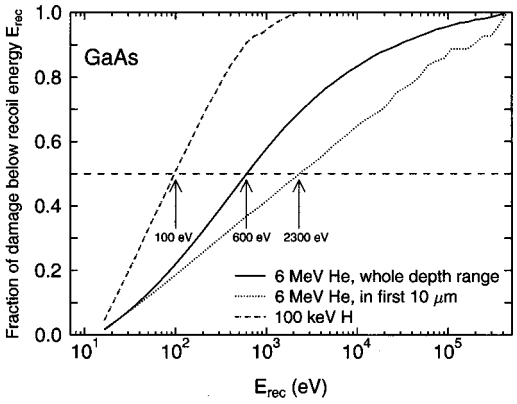

FIG. 6. Fraction of total damage produced by primary recoils with energies below E_{rec} during 100 keV H and 6 MeV He ion irradiation of GaAs, evaluated by a combined MD range calculation and MD cascade simulations is shown.

The recoil spectra $n_t(E)dE$ are illustrated in Fig. 5 and the fraction of damage produced by recoils up to a given energy E in Fig. 6. Figure 5 shows the number of primary recoils produced per ion as a function of energy, integrated over either the whole depth range or the first 10 μm. Now by performing the integral in Eq. (1), one obtains the total damage produced by the high-energy irradiation (see Sec. II B). By integrating to E instead of E_0, and normalizing to the total damage production, one obtains the fraction of damage below a given primary recoil energy. This gives the curves in Fig. 6.

A quantitative measure at which recoil energies dominate the energy production is the primary recoil energy at below which half of the damage energy is deposited, $T_{1/2}$ (Ref. 26). The values for $T_{1/2}$ are 600 eV for recoils in the whole depth range, and 2300 eV for recoils in the first 10 μm. Thus, we reach the conclusion that in the first 10 μm most of the damage is produced by higher-energy recoils than in the whole irradiation range.

The defect numbers given in Table II show that this difference does not effect the relative number of damage in clusters much, however. Both for the whole depth range and the first 10 μm, roughly 80% of the vacancies and 70% of the interstitials are in clusters. This is because for both kinds of defects, at least 70% of the damage is produced by recoils above 400 eV, and, already at this energy, much of the damage is in clusters.

The 100 keV H irradiation, however, does behave differently. Only about 50% of the damage is in clusters. This is because for this ion, 50% of the damage is produced by recoils below 100 eV, where defect clustering is not yet that significant.

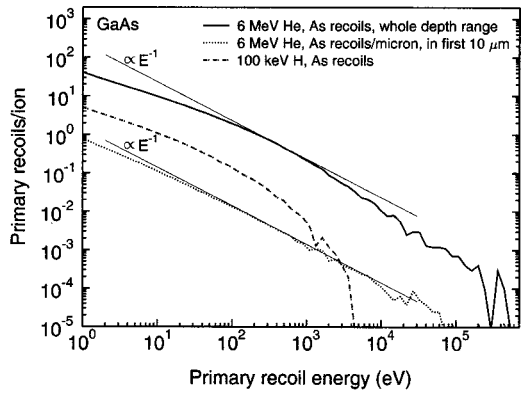

FIG. 5. Average number of primary As recoils produced per ion during 100 keV H and 6 MeV He ion irradiation of GaAs is shown. The numbers of Ga recoils are not shown since these overlap almost exactly the As curves. The thin lines indicate an E^{-1} energy behavior.

C. Antisites

The interesting issue for many experimental situations is how much of the damage remains at room temperature or higher. Especially interesting is the number of antisites produced, since this defect is stable up to high temperatures and has interesting electrical properties.[27]

The simulations just described are directly valid only for temperatures below those where any kind of annealing occurs. TEM experiments, however, show that even very large

TABLE II. Damage produced by 100 keV H and 6 MeV He irradiation of GaAs per incoming ion is shown. The results for 6 MeV He are given for the whole ~24 μm implantation range, and in the first 10 μm reported as damage per 1 μm. The upper part of the table gives the total number of vacancies (vac.) and interstitials (int.), and how many of these are in clusters. The number of free defects can be obtained by subtracting these two numbers. Since the nuclear energy deposition profile is essentially flat in the region 0–10 μm, the damage per micron can be expected to be about the same anywhere in this depth range. The table lists Wigner–Seitz defects; since more than two atoms can, in rare instances, be in the same Wigner–Seitz cell, the number of interstitials is slightly lower than the number of vacancies.

		6 MeV He	
Type of Damage	100 keV H (defects/ion)	All z (defects/ion)	First 10 μm (defects/μm/ion)
Vac.	10.9±0.2	297±4	2.85±0.04
Int.	10.6±0.1	289±3	2.77±0.04
Clustered vac.	6.1±0.2	231±4	2.30±0.04
Clustered int.	5.1±0.2	191±4	1.90±0.04
Clusters	1.6±0.1	62±1	0.62±0.01
Large clusters	0.23±0.03	13±1	0.14±0.01
Antisites	0.84±0.03	23±1	0.22±0.01

amorphous clusters anneal completely over a few minutes at room temperature.[12,13] It is not known what damage remains at the site of the amorphous cluster, since TEM experiments can not see defects smaller than about 1 nm.

Since at least some of the possible interstitial and vacancy configurations in GaAs are mobile at room temperature,[28,27] it is not possible within the limited time scale of MD simulations to predict how the annealing actually occurs. However, it is possible to estimate roughly how much damage can be expected to remain by a rapid heating of the cell. To be precise, we heated the cells to 1000 K for 100 ps and subsequently quenched them back to 0 K to enable accurate defect recognition. This allows us to estimate the number of antisites remaining after recrystallization. Since antisites are neither experimentally mobile at room temperature,[27] nor have time to anneal or migrate during the quick heating of our simulation cell, our simulations should provide an estimate of their numbers after the amorphous clusters have annealed.

We found that, as for the other defects, the number of antisites produced is linear with energy, so we can calculate their number produced in the H and He irradiation similarly as for the other defects. The result is given in Table II.

The number of antisites is small, more than an order of magnitude smaller than the number of defects prior to annealing. This conclusion is in good agreement with previous simulations employing lower-energy recoils.[5] However, since the amorphous zones anneal out at room temperature, and much of the remaining damage is in small clusters, many of which can also be expected to anneal out easily,[29] the antisites will be one of the most important defects remaining at high temperatures.

IV. DISCUSSION

A. Damage production in cascades

The linear dependence of the amount of damage produced with the incoming ion energy is similar to the behavior that has been observed in Si and Ge before.[8,30] It is, however, in stark contrast to the behavior in metals, where a dramatic drop of the defect production efficiency is observed with increasing energy.[26] The linear behavior in Si and Ge has been explained to be due to the poor ability of the open diamond lattice structure to regenerate the lattice from molten zones, and hence it is not surprising that the same behavior is observed in GaAs.[6,31]

The linear behavior also essentially implies that the simple modified Kinchin–Pease[32] estimate for the total number of Frenkel pairs produced N_{FP},

$$N_{\mathrm{FP}} = 0.8 \frac{F_{D_n}}{2E_d} \tag{2}$$

is valid in GaAs. Here E_d is the average displacement energy of the material. From the fitting constant used in describing the total number of vacancies, we obtain from our MD simulations a value of $E_d = 14.8 \approx 15$ eV.

Overall, the cascades in GaAs behave much like cascades in Ge, which we have studied earlier.[8] The total number of defects produced is similar at all the energies. In Ge, we found that about 40% of the defects produced at 400 eV, and about 90% of those produced at higher energies, were in large (at least six defects) clusters. In GaAs, the fraction of clustered defects is almost exactly the same at 400 eV, but only about 60% at higher energies. Also, at the highest energies simulated, we observed somewhat (about 30%) larger total numbers of defects in Ge. The likely reason for this difference is that the lower melting point of Ge (1200 K) compared to GaAs (1500 K) allows for the production of larger amorphous zones. This observation is in excellent agreement with TEM experiments, in which amorphous zones in Ge have also been observed to be somewhat larger than those in GaAs.[33,34]

It is not possible to make an exact comparison between experimental and simulated displacement energies, as different definitions of what is a defect both in simulations and experiments give conflicting values, and the correspondence between simulated and experimental quantities is not known. Nevertheless, the displacement energy obtained from Wigner–Seitz defects is reasonable for a rough comparison with the experiment, as the Wigner–Seitz analysis will always give exactly one displaced atom for an isolated Frenkel pair, which follows the usual definition.

Experimentally, there has been some uncertainty in the value of the displacement energy in GaAs. Some early sources reported *threshold* (minimum) displacement values around 25 eV,[35] but most recent sources report values close to 10 eV.[28,36–38] We could not find a value for the *effective* (average) displacement energy measured using nonelectrical methods at low temperatures, to which our displacement value would correspond. But since the effective displacement energy is typically somewhat ($\sim$50%) higher than the threshold one,[39,32] the value of 15 eV seems very reasonable in comparison to the experiment.

These observations imply that simple BCA models (such as TRIM)[17,40] can be used to obtain quick estimates of the total amount of damage produced in GaAs, with a threshold displacement energy of 15 eV.

B. Damage by high-energy recoils

We saw that the damage produced in the near-surface region is produced by somewhat higher-energy recoils than those in the whole depth range. To estimate how big an effect this has on the typical cluster sizes, we calculated the actual number of clusters, in the same way as the number of defects was calculated. The results are listed in Table II. We calculated both the total number of clusters, and the number of large clusters. A large cluster is one with at least six defects; this is of course a quite arbitrary limit. The numbers do, however, show that the ratio between the number of all clusters and large clusters is about the same for the whole range and the surface region. This shows that even in the surface regions, some very large damage clusters will be present.

After annealing, which experimentally occurs even at room temperature, the amorphous zones vanish, and the remaining damage is mostly in isolated defects, small defect clusters, and antisites. At least the antisites will be stable up

to very high temperatures, and may thus seriously degrade the performance of GaAs devices in space.

V. CONCLUSIONS

We have studied point defect and defect cluster production in GaAs by self-recoils and high-energy light ions using MD simulations. We showed that even for low-energy (400 eV) recoils, about half of the damage produced is in large clusters containing at least six defects. For 100 keV H and 6 MeV He irradiation of GaAs, we showed that although most of the damage is near the ion end of range, very large damage clusters can be expected to be produced throughout the ion range. We demonstrated that a sizable number of antisites can be expected to remain after annealing even in the near-surface regions, where damage levels are often assumed to be low.

ACKNOWLEDGMENTS

The authors thank Dr. J. U. Patel and E. Hollar for useful discussions. The research was supported by the Academy of Finland under Project Nos. 44215 and 46788, the U.S. Department of Energy, Basic Energy Sciences, under Grant No. DEFG02-91ER45439, and NASA Jet Propulsion Laboratory. Grants of computer time from the Center for Scientific Computing in Espoo, Finland are gratefully acknowledged.

APPENDIX A: POTENTIAL FUNCTION

The potential we use for GaAs was developed by K. Albe in collaboration with our group. The potential is described in greater detail elsewhere,[11] so we only describe the central features here. The potential is based on the Tersoff formalism; however, we found it necessary to modify the λ_3 term[41] for compounds to prevent very strong forces when nonequivalent atoms are in the potential cutoff region. The resulting potential form is essentially the same as that of the Brenner potential excluding the functions describing bond conjugation.[42] The potential correctly reproduces the ground states of Ga, As, and GaAs; this is important to prevent the collapse of GaAs into artificial states when it is molten for instance in collision cascades. It also gives a reasonably good value for the melting point of GaAs (1900 K, vs the experimental value of 1510 K).[43] It was fitted to reproduce all the first-order elastic constants of GaAs, as well as several over- and under-coordinated phases. We believe these features make the potential well suited for studies of irradiation effects, at least for robust effects such as defect distribution, disordering, and amorphization.

We write the potential energy as a sum over individual bond strengths:

$$V_{\mathrm{Eq}}=\sum_{i>j} f_{ij}(r_{ij})\left[V_{ij}^{R}(r_{ij})-\frac{B_{ij}+B_{ji}}{2}V_{ij}^{A}(r_{ij})\right]. \tag{3}$$

Here, the pair-like attractive and repulsive energies are given in a Morse-type form,

$$V^{R}(r)=\frac{D_e}{S-1}\exp[-\beta\sqrt{2S}(r-R_e)], \tag{4}$$

$$V^{A}(r)=\frac{SD_e}{S-1}\exp[-\beta\sqrt{2/S}(r-R_e)],$$

where D_e and R_e are the dimer bond energy and distance, and S and β are adjustable parameters.

The cutoff function f_{ij} is used to restrict the interaction to the next neighbors and is defined as:

$$f(r)=\begin{cases}1, & r\leqslant R_{\mathrm{cut}}-D_{\mathrm{cut}},\\ \frac{1}{2}-\frac{1}{2}\sin\{\pi(r-R_{\mathrm{cut}})/(2D_{\mathrm{cut}})\}, & |R_{\mathrm{cut}}-r|\leqslant D_{\mathrm{cut}},\\ 0, & r\geqslant R_{\mathrm{cut}}+D_{\mathrm{cut}},\end{cases} \tag{5}$$

with D_{cut} and R_{cut} as adjustable parameters. The many-body term is adopted from Brenner and is formulated as:

$$B_{ij}=(1+\chi_{ij})^{-1/2},$$
$$\chi_{ij}=\sum_{k(\neq i,j)} f_{ik}(r_{ik})g_{ik}(\theta_{ijk})\exp[2\mu_{ik}(r_{ij}-r_{ik})], \tag{6}$$

where the angular function $g(\theta)$ is

$$g(\theta_{ijk})=\gamma\left(1+\frac{c^2}{d^2}-\frac{c^2}{[d^2+(h+\cos\theta_{ijk})^2]}\right). \tag{7}$$

To realistically account for high-energy ($E_{\mathrm{kin}}\gg 10$ eV) collisions, we construct a total potential V_{Tot} using

$$V_{\mathrm{Tot}}(r)=V_R(r)[1-F(r)]+[V_{\mathrm{Eq}}(r)]F(r), \tag{8}$$

where V_{Eq} is the potential for states close to equilibrium described, $V_R(r)$ is the repulsive pair potential for close interactions and the Fermi function

$$F(r)=\frac{1}{1+e^{-b_f(r-r_f)}}. \tag{9}$$

The repulsive potential $V_R(r)$ is derived from density-functional theory calculations.[44–46] The value of the constants b_f and r_f are chosen such that the potential is essentially unmodified at the equilibrium and longer bonding distances, and that a smooth fit to the repulsive potential at short separations with no spurious minima is achieved for all realistic coordination numbers. We emphasize that in appli-

TABLE III. Full parameter set for the three types of interactions is shown.

ij	Ga–Ga	As–As	Ga–As
γ	0.007 874	0.455	0.0166
S	1.11	1.86	1.1417
$\beta(\text{Å}^{-1})$	1.08	1.435	1.5228
D_e(eV)	1.40	3.96	2.10
R_e(Å)	2.3235	2.10	2.35
c	1.918	0.1186	1.29
d	0.750	0.1612	0.56
$h=\cos(\theta_0)$	0.3013	0.077 48	0.237
$\mu(\text{Å}^{-1})$	1.846	3.161	0.0
R_{cut} (Å)	2.95	3.4	3.1
D_{cut} (Å)	0.15	0.2	0.2
r_f (Å)	1.2	1.0	1.0
$b_f(\text{Å}^{-1})$	12.0	12.0	12.0

cations where high-energy collisions are not present, there is no need to include the high-energy repulsive potential. The parameter values are given in Table III.

[1] J. W. Mayer and S. S. Lau, *Electronic Materials Science for Integrated Circuits in Si and GaAs* (MacMillan, New York, 1990).
[2] T. Diaz de la Rubia, R. S. Averback, R. Benedek, and W. E. King, Phys. Rev. Lett. **59**, 1930 (1987).
[3] M. Ghaly and R. S. Averback, Phys. Rev. Lett. **72**, 364 (1994).
[4] T. Diaz de la Rubia and G. H. Gilmer, Phys. Rev. Lett. **74**, 2507 (1995).
[5] T. Mattila and R. N. Nieminen, Phys. Rev. Lett. **74**, 2721 (1995).
[6] M.-J. Caturla, L. A. M. T. Diaz de la Rubia, and G. H. Gilmer, Phys. Rev. B **54**, 16683 (1996).
[7] H. Hensel and H. M. Urbassek, Phys. Rev. B **57**, 4756 (1998).
[8] K. Nordlund, M. Ghaly, R. S. Averback, M. Caturla, T. Diaz de la Rubia, and J. Tarus, Phys. Rev. B **57**, 7556 (1998).
[9] M. Sayed, J. H. Jefferson, A. B. Walker, and A. G. Gullis, Nucl. Instrum. Methods Phys. Res. B **102**, 232 (1995).
[10] K. Nordlund, J. Nord, J. Frantz, and J. Keinonen, Comput. Mater. Sci. **18**, 283 (2000).
[11] K. Albe, K. Nordlund, and J. Nord, *Modeling of Compound Semiconductors: Analytical Bond-Order Potential for GaAs* (to be published).
[12] M. W. Bench, I. M. Robertson, and M. A. Kirk, Nucl. Instrum. Methods Phys. Res. B **59**, 372 (1991).
[13] M. W. Bench, I. M. Robertson, M. A. Kirk, and I. Jenčič, J. Appl. Phys. **87**, 49 (2000).
[14] D. M. Scott and D. C. Marvin, *Conference Record of the Twenty Third IEEE Photovoltaic Specialists Conference* (IEEE, New York, 1993), p. 1338.
[15] H. J. C. Berendsen, J. P. M. Postma, W. F. van Gunsteren, A. DiNola, and J. R. Haak, J. Chem. Phys. **81**, 3684 (1984).
[16] K. Nordlund, Comput. Mater. Sci. **3**, 448 (1995).
[17] J. F. Ziegler, J. P. Biersack, and U. Littmark, *The Stopping and Range of Ions in Matter* (Pergamon, New York, 1985).
[18] J. F. Ziegler, SRIM-96 computer code, 1996 (private communication).
[19] A. Luukkainen and M. Hautala, Radiat. Eff. **59**, 113 (1982).
[20] J. Nord, K. Nordlund, and J. Keinonen, *Modeling of Amorphization of Semiconductors* (to be published).
[21] P. Haussalo, K. Nordlund, and J. Keinonen, Nucl. Instrum. Methods Phys. Res. B **111**, 1 (1996).
[22] K. Nordlund, J. Keinonen, and T. Mattila, Phys. Rev. Lett. **77**, 699 (1996).
[23] J. Sillanpää, K. Nordlund, and J. Keinonen, Phys. Rev. B **62**, 3109 (2000).
[24] J. Nord, K. Nordlund, and J. Keinonen (unpublished).
[25] K. Nordlund, J. Nord, and J. Keinonen, Nucl. Instrum. Methods (accepted for publication).
[26] R. S. Averback and T. Diaz de la Rubia, in *Solid State Physics*, edited by H. Ehrenfest and F. Spaepen (Academic, New York, 1998), Vol. 51, pp. 281–402.
[27] S. Kuisma, K. Saarinen, P. Hautojarvi, and C. Corbel, Phys. Rev. B **55**, 9609 (1997).
[28] H. Hausmann, A. Pillukat, and P. Ehrhart, Phys. Rev. B **54**, 8527 (1996).
[29] K. S. and S. Kuisma, J. Mäkinen, P. Hautojärvi, M. Törnqvist, and C. Corbel, Phys. Rev. B **51**, 14152 (1995).
[30] J. Tarus, K. Nordlund, A. Kuronen, and J. Keinonen, Phys. Rev. B **58**, 9907 (1998).
[31] K. Nordlund and R. S. Averback, Phys. Rev. B **56**, 2421 (1997).
[32] M. Nastasi, J. Mayer, and J. Hirvonen, *Ion-Solid Interactions—Fundamentals and Applications* (Cambridge University Press, Cambridge, UK, 1996).
[33] I. Jencic, M. W. Bench, I. M. Robertson, and M. A. Kirk, J. Appl. Phys. **78**, 974 (1995).
[34] M. W. Bench, Ph.D. thesis, University of Illinois at Urbana- Champaign, 1992.
[35] A. H. Kalma, R. A. Berger, C. J. Fischer, and B. A. Green, IEEE Trans. Nucl. Sci. **22**, 2277 (1975).
[36] A. L. Barry, R. Maxseiner, R. Wojcik, M. A. Briere, and D. Braunig, IEEE Trans. Nucl. Sci. **37**, 1726 (1990).
[37] B. Lehmann and D. Braunig, J. Appl. Phys. **73**, 2781 (1993).
[38] D. A. Thompson, Radiat. Eff. **56**, 105 (1981); and references therein.
[39] H. H. Andersen, Appl. Phys. **18**, 131 (1979).
[40] J. P. Biersack and L. G. Haggmark, Nucl. Instrum. Methods **174**, 257 (1980).
[41] J. Tersoff, Phys. Rev. B **37**, 6991 (1988).
[42] D. W. Brenner, Phys. Rev. B **42**, 9458 (1990); *idem*. **46**, 1948 (1992).
[43] J. A. V. Vechten, Phys. Rev. B **7**, 1479 (1973).
[44] J. Delley, J. Chem. Phys. **92**, 508 (1990).
[45] K. Nordlund, N. Runeberg, and D. Sundholm, Nucl. Instrum. Methods Phys. Res. B **132**, 45 (1997).
[46] The repulsive potential data are available by E-mail request from kai.nordlund@helsinki.fi.